ACS APPLIED MATERIALS & INTERFACES

Research Article

www.acsami.org

Photoinduced Charge Transfer Properties and Photocatalytic Activity in $Bi_2O_3/BaTiO_3$ Composite Photocatalyst

Haimei Fan,[†] Haiyan Li,[‡] Bingkun Liu,[†] Yongchun Lu,[†] Tengfeng Xie,*[,†] and Dejun Wang*[,†]

[†]State Key Laboratory of Theoretical and Computational Chemistry, College of Chemistry, Jilin University, Changchun 130012, China

[‡]State Key Laboratory of Electroanalytical Chemistry, Changchun Institute of Applied Chemistry, Chinese Academy of Sciences, Changchun 130022, China

ABSTRACT: A series of $Bi_2O_3/BaTiO_3$ composite photocatalysts with different mass ratios of Bi_2O_3 vs $BaTiO_3$ were prepared by an impregnating-annealing method. X-ray diffraction (XRD), high-resolution transmission electron microscopic (HRTEM), and UV−vis diffuse reflection spectroscopy (DRS) confirmed that Bi_2O_3 and $BaTiO_3$ coexisted in the composites. The results of surface photovoltage (SPV) experiments showed enhancements of photovoltaic response in composites, which indicated a higher separation efficiency of photoinduced charges due to the establishment of an efficient interfacial electric field between Bi_2O_3 and $BaTiO_3$ in the composites. The consistency of phtocatalytic activity and photovoltaic response intensity of photocatalysts showed that the efficiency interfacial electric field between Bi_2O_3 and $BaTiO_3$ played an important role in improving the degradation efficiency of Rhodamine B (RhB). The 60%-$Bi_2O_3/BaTiO_3$ sample with the best activity was found by optimizing the mass ratios of Bi_2O_3 vs. $BaTiO_3$. On the basis of the work function (WF) measurements, a reasonable energy band diagram was proposed for $BaTiO_3/Bi_2O_3$ composite. It would be helpful in designing and constructing high efficiency heterogeneous semiconductor photocatalyst.

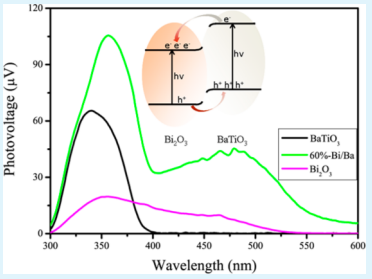

KEYWORDS: *$Bi_2O_3/BaTiO_3$ composite, photocatalytic, photovoltage, charge transfer, work function, interface*

1. INTRODUCTION

Semiconductor photocatalysts, which hold great potential for converting solar energy to chemical energy, have been proven to be available and promising materials for environmental purification.[1,2] The key to enhancing the photocatalytic activity of semiconductor mainly lies in effectively combining the photon absorption, bulk diffusion and the separation of photoinduced charge.[3] Unfortunately, most semiconductor oxides generally have a wide band gap and relatively high recombination rate of electron-hole pairs, leading to a poor efficiency of photocatalytic reaction. Therefore, a variety of approaches have been explored to enhance the quantum yield of semiconductors, including phase/morphological control, ion doping, surface sensitization, noble metal loading, and heterostructure constructing.[4]

Semiconductor composite, which constructs a heterojunction interface between two types of semiconductor with matching energy levels, can facilitate the interfacial charge transfer and enhance the separation of photoinduced charges. For the above reason, it has attracted increasing attention in recent years. So far, variety semiconductor heterojunction including CdS/TiO_2,[5] $FeTiO_3/TiO_2$,[6] CdS/ZnO,[7] $CuBi_2O_4/WO_3$,[8] $Co_3O_4/BiVO_4$,[9] Bi_2O_3/Bi_2O_{4-x},[10] have been reported as photocatalysts. Huang et al. have reported the $BiVO_4$@Bi_2O_3 microspheres photocatalyst with high photocatalytic activity in degradation rhodamine B (RhB) under visible-light irradiation.[11] Fu and co-workers have prepared $LaVO_4/TiO_2$ nanocrystalline photocatalyst which exhibited strong photocatalytic activity for decomposition of benzene under visible light irradiation.[12] They considered that the enhancement of photocatalytic activity should be attributed to the formation of heterostruture. Lin et al. have prepared $Bi_2O_3/BaTiO_3$ heterojunction semiconductors and proposed a strategy for the design of efficient composite photocatalysts.[13] However, there are few reports about detailed explanation of the transfer behavior of photoinduced charges in semiconductor composite including separation, transfer, and recombination. A better understanding of the above information will provide deep insight into the intrinsic reasons of enhancement in photocatalytic activity. In view of these, we intended to prepare $Bi_2O_3/BaTiO_3$ composites that have matched band potentials, and used it as a model to study the character of photoinduced charge at the composite.

In this work, the $Bi_2O_3/BaTiO_3$ composite photocatalysts were prepared and exhibited much better photocatalytic activity than that of single Bi_2O_3 or $BaTiO_3$. The surface photovoltage (SPV) experiment and work function (WF) measurements were used to investigate photovoltaic properties of the samples.

2. MATERIAL AND METHODS

2.1. Catalyst Preparation. All the chemicals were analytical grade and used as received without further purification. The $BaTiO_3$ samples

Received: July 1, 2012
Accepted: August 24, 2012
Published: August 24, 2012

   dx.doi.org/10.1021/am301199v | *ACS Appl. Mater. Interfaces* 2012, 4, 4853−4857

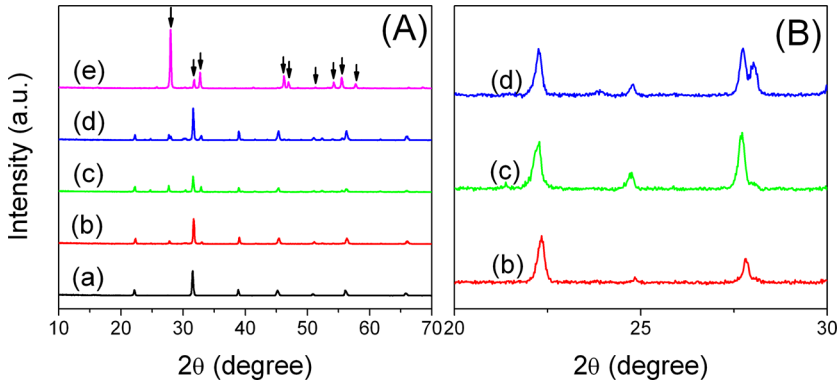

Figure 1. (A) XRD patterns of the as-prepared samples with different $Bi_2O_3/BaTiO_3$ mass ratio. (a) $BaTiO_3$, (b) 30% $Bi_2O_3/BaTiO_3$, (c) 60% $Bi_2O_3/BaTiO_3$, (d) 90% $Bi_2O_3/BaTiO_3$, (e) Bi_2O_3, and x% refers to the mass ratio of $Bi_2O_3/BaTiO_3$. (down arrows indicate Bi_2O_3); (B) higher magnification of A in the range of 20−30°.

were synthesized using Degussa P-25 TiO_2 by a hydrothermal process (180 °C, 24 h) reported by Chen et al.[14] The prepared $BaTiO_3$ samples (0.3 g) were then added to 15 mL of ethanol aqueous containing a certain amount of $Bi(NO_3)_3{\cdot}5H_2O$ (≥99.0%; Shanghai Zhenxin Chemical Works). The amounts of $Bi(NO_3)_3{\cdot}5H_2O$ were 0.09, 0.18, and 0.27 g, respectively, for the 30, 60, and 90% composites. The suspension was sonicated to evenly mix, after being dried, the composite powders were heat-treated at 700 °C for 2 h in an oven.[13] The as-prepared samples were expressed as *x*% $Bi_2O_3/BaTiO_3$, in which *x*% refers to the mass ratio of $Bi_2O_3/BaTiO_3$.

2.2. Photocatalytic Activity Test. Photodegradation studies of RhB were carried out in a homemade quartz photochemical reactor. Before light irradiation, 0.025 g of photocatalyst was added into 25 mL of rhodamine B (RhB) aqueous solution (10 mg/L). The mixture was first sonicated for 5 min and then kept in the dark for 1 h with stirring to reach the adsorption−desorption equilibrium. The visible light source was a 500 W Xenon lamp (CHFXQ500 W) with a UV filter. The UV light source was a 500 W mercury lamp. At the given time intervals, analytical samples were taken from the suspension and immediately centrifuged at 10000 rpm for 5 min. The concentration analysis of RhB was determined by using an Ocean Optics Miniature Fiber Optic Spectrometer (Maya 2000).

2.3. Methods. The crystalline phase was examined by X-ray diffraction (XRD) using a Rigaku D/Max-2550 diffractometer with Cu K_α radiation (λ = 1.54056 Å) at 50 kV and 200 mA in the range of 10-70° (2θ) at a scanning rate of 10° min^{-1}. The UV−-vis diffuse reflectance spectra were recorded with a Shimadzu (UV-3600) UV−Vis−NIR spectrophotometer. The high-resolution transmission electron microscopic (HRTEM) imaging was performed on a TECNAIG^2 TEM microscope (FEI Company).

The SPV measurement system consisted of a source of monochromatic light, a lock-in amplifier (SR830-DSP) with a light chopper (SR540), a photovoltaic cell, and a computer. A 500 W xenon lamp (CHFXQ500 W, Global Xenon Lamp Power) and a double-prism monochromator (Hilger and Watts, D 300) provided monochromatic light. The samples were studied without further treatment during the SPV measurements, and the contact between samples and the indium tin oxide (ITO) electrode was not Ohmic when carried out the measurement of surface photovoltage. The construction of the photovoltaic cell was a sandwich-like structure of ITO−sample−ITO.

Work function measurements were carried out on a commercial scanning Kelvin probe system (KP Technology Ltd., Scotland, UK). The width of the gold reference probe was 1.8 mm, whose work function was 5.1 eV. The contact potential difference (CPD) between the sample and the probe was measured in dark.

3. RESULTS AND DISCUSSION

Figure 1 showed the XRD patterns of $Bi_2O_3/BaTiO_3$ samples with different mass ratio. For pure $BaTiO_3$, all the peaks can be well indexed to the tetragonal phase (JCPDS File No. 05-0626) and the pure Bi_2O_3 was the β-Bi_2O_3 (JCPDS File No. 78-1793). For $Bi_2O_3/BaTiO_3$ composite, there were two sets of diffraction peaks, which were correspondingly ascribed to $BaTiO_3$ and β-Bi_2O_3. No other characteristic peaks were detected indicating that the as-prepared composites consisted of the tetragonal $BaTiO_3$ and β-Bi_2O_3 and no appreciable chemical reaction occurred between $BaTiO_3$ and $Bi(NO_3)_3$ during the calcination process at 700 °C. In Figure 1B, the peak area ratio of 28° for Bi_2O_3 to 22.3 of $BaTiO_3$ were 0.4, 0.9, and 1.4, respectively, for 30, 60, and 90% composite, which indicated that the amount of Bi_2O_3 increased with the increasing of its addition.

TEM and HRTEM were used to study the morphology and microstructure of $Bi_2O_3/BaTiO_3$ composite. A low magnification TEM image was shown in Figure 2a, from which we can see that the Bi_2O_3 nanoparticles with the size of 3−10 nm mutually aggregated on the surface of $BaTiO_3$. The

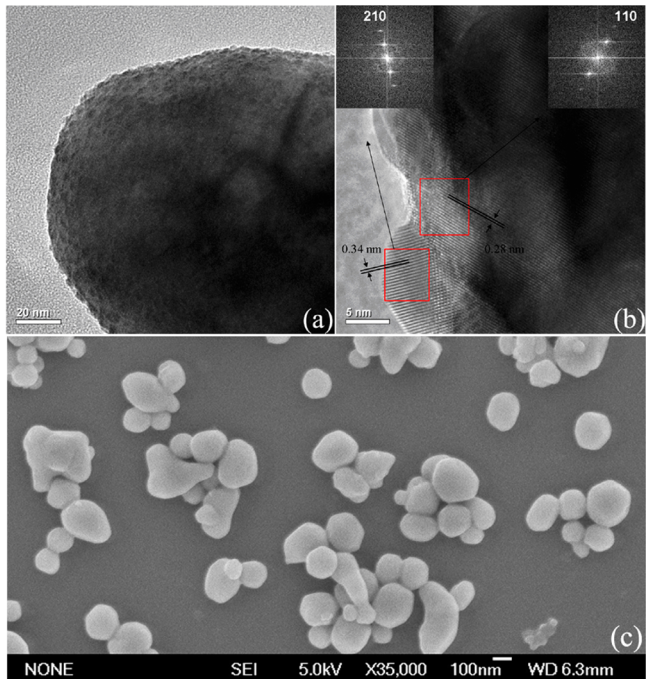

Figure 2. (a) TEM image and (b) HRTEM image of 60% $Bi_2O_3/BaTiO_3$ composite. The insets in b are FFT patterns. (c) SEM of $BaTiO_3$.

representative HRTEM image in Figure 2b showed the lattice fringes of $Bi_2O_3/BaTiO_3$ and fast Fourier transform (FFT) analysis was conducted on a selected area of 60% $Bi_2O_3/BaTiO_3$ in Figure 2b, which was displayed in the insets. In the upper-left inset, the *d* spacing of (210) was 0.34 nm, which was in good agreement with that of β-Bi_2O_3.[15] In the upper-right inset, the *d* spacing of (110) was 0.28 nm, which matched well with that of tetragonal $BaTiO_3$.[16] The above results indicated that the nanostructured composite consisted of Bi_2O_3 and $BaTiO_3$.

The UV−vis diffuse reflectance spectra of the as-prepared powders were shown in Figure 3. The band gap of $BaTiO_3$ and

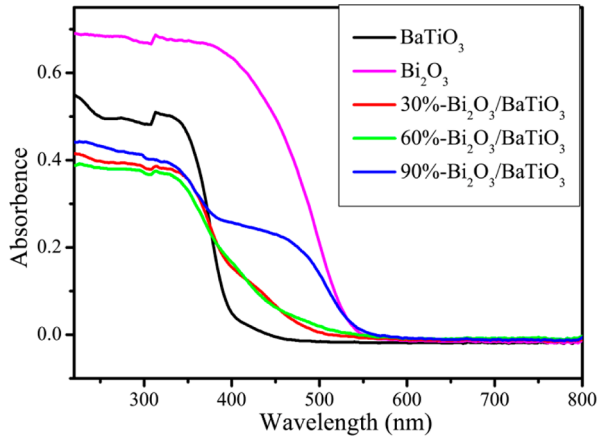

Figure 3. UV−vis diffuses reflectance spectra of $BaTiO_3$, Bi_2O_3, and the $Bi_2O_3/BaTiO_3$ composites with different mass ratio.

Bi_2O_3 were estimated to be 3.18 and 2.39 eV, respectively, which were consistent with the literature.[17,18] The optical absorption of $Bi_2O_3/BaTiO_3$ composite powders started at about 520 nm, which was caused by the existence of Bi_2O_3. And with the increasing of Bi_2O_3 content, absorbance intensity of composite increased under visible light. Two absorption edges are observed for the adsorption spectra of $BaTiO_3/Bi_2O_3$ composite powder when the content of Bi_2O_3 reached to 90%.

We comparatively investigated the transfer properties of photoinduced charges at the surface or interface of the pure Bi_2O_3, pure $BaTiO_3$ and $Bi_2O_3/BaTiO_3$ composites powder by using SPV technique, which can provide a rapid and direct investigation of the band-gap transition.[19,20] And the result was shown in Figure 4. For single Bi_2O_3 and $BaTiO_3$ samples, the SPV response bands were obtained in the range of 300−520 nm and 300−380 nm, respectively, which were due to the band−band transition (electrons transition from valence band to conduction band). There was no any SPV response for $BaTiO_3$ under the irradiation of visible light. However, $Bi_2O_3/BaTiO_3$ composites displayed a similar SPV response range (from 300 nm to 520 nm) to Bi_2O_3 suggesting that the photovoltage response of composite in the visible region mainly resulted from Bi_2O_3.[21] Under the visible irradiation, the response intensity of pure Bi_2O_3 was stronger than the response intensity of 30% $Bi_2O_3/BaTiO_3$ composite but weaker than the response intensity of 60 and 90% $Bi_2O_3/BaTiO_3$ composite. In the UV response region, the SPV response intensity of composite was not the simple addition of pure $BaTiO_3$ and Bi_2O_3. The response intensity of $BaTiO_3$ was stronger than that of 30 and 90% $Bi_2O_3/BaTiO_3$ composite but weaker than the response intensity of 60% $Bi_2O_3/BaTiO_3$

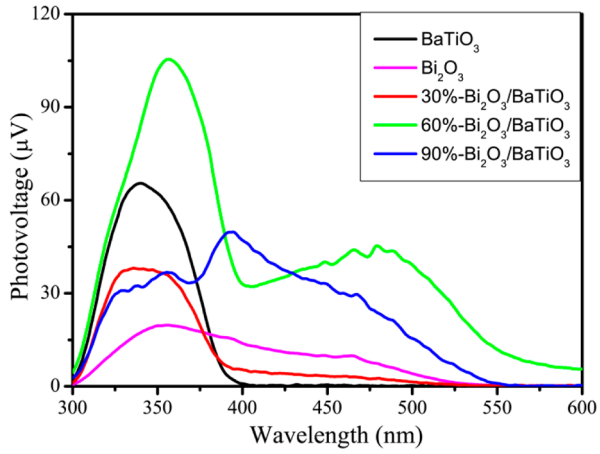

Figure 4. SPV spectra of Bi_2O_3, $BaTiO_3$, and $Bi_2O_3/BaTiO_3$ composites with different mass ratio.

composite. Unlike the UV−vis spectra, which covered all types of photon absorption, the SPV was only sensitive to the electron transition-related process and subsequent separation. On this basis, the photovoltage response intensity was related to the charge separation efficiency, which signified that a stronger SPV response intensity, a higher separation efficiency of photoinduced charges.[22,23] The SPV result implied the 60% $Bi_2O_3/BaTiO_3$ composite had a higher separation efficiency of photoinduced charges than that of pure Bi_2O_3 or pure $BaTiO_3$. We speculated that there was an interfacial electric field in $Bi_2O_3/BaTiO_3$ composite due to the addition of Bi_2O_3 during the calcination process. The penetrating depth of visible may reach to the interface of Bi_2O_3 and $BaTiO_3$, so the interfacial electric field may play a dominant role on the separation of photoinduced charges. The response intensity 60% $Bi_2O_3/BaTiO_3$ composite was higher than pure Bi_2O_3 because the existence of interfacial electric field enhances the separation of photoinduced charges. However, 30% $Bi_2O_3/BaTiO_3$ composite had a smaller amount of Bi_2O_3 resulting in a weaker absorption in the visible light, so there was a weaker SPV response intensity. When the mass ratio reached to 90%, agglomeration of the Bi_2O_3 particles resulted in a reducing of photons reached to the interface and an increasing of migration distance of photoinduced charges. So the response intensity of 90% $Bi_2O_3/BaTiO_3$ composite was weaker than the intensity of 60% $Bi_2O_3/BaTiO_3$ composite.

Figure 5 showed the SPV result of mechanical mixed Bi_2O_3 and $BaTiO_3$ with the ratio of 60% (the mass ratio of Bi_2O_3 is 60% and without any calcination). The SPV response intensity of the mechanical mixture was much lower than that of 60% $Bi_2O_3/BaTiO_3$ composite which indicated that photoinduced charge separation of in composite was much easier than that in the mechanical mixed Bi_2O_3 and $BaTiO_3$. This result further confirmed the existence of interfacial electric field.

In order to evaluate the photocatalytic ability of $Bi_2O_3/BaTiO_3$, we examined the decomposition of RhB dye in solution over the $BaTiO_3$, Bi_2O_3 and $Bi_2O_3/BaTiO_3$ composite with different mass ratio under the irradiation of UV light and visible light (λ > 400 nm). The results were shown in Figure 6.

From Figure 6, we can see that both Bi_2O_3 and $BaTiO_3$ showed a very low photocatalytic activity, while $Bi_2O_3/BaTiO_3$ composite demonstrated notably high activity. This result was consistent with the speculation of the SPV result. It was deduced that the high photocatalisis efficiency of the $Bi_2O_3/$

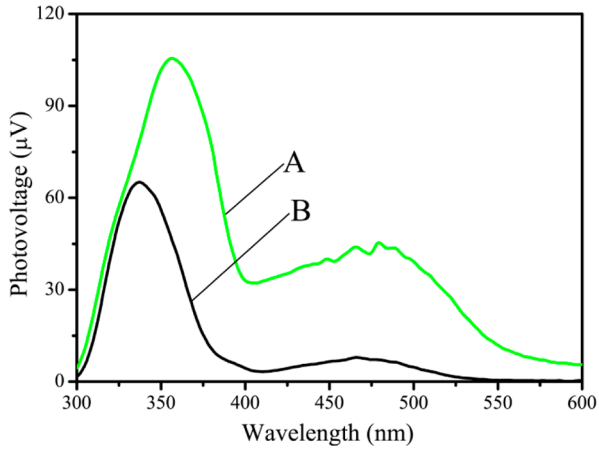

Figure 5. SPV spectra of (A) 60% Bi_2O_3/$BaTiO_3$ composite and (B) mechanical mixture Bi_2O_3 and $BaTiO_3$ with the ratio of 60% (the mass ratio of Bi_2O_3 is 60% without any calcination).

$BaTiO_3$ composite originates from the unique relative band positions and effective interface contacting these two semiconductors.

HRTEM showed the compact contacted between Bi_2O_3 and $BaTiO_3$ in the composite and the SPV result gave other evidence for the existence of interfacial electric field; however, how did it form and affect the charge-transfer process? To understand this process, we should consider the electronic structure of Bi_2O_3 and $BaTiO_3$. The conduction band (CB) and valence band (VB) positions of the two semiconductors at the point of zero charge are predicted theoretically by eq 1

$$E_{CB}^{0} = X - E^{c} - 1/2E_{g} \quad (1)$$

Where X was the absolute electronegativity of the semiconductor, expressed as the geometric mean of the absolute electronegativity of the constituent atoms; E^c was the energy of free electrons on the hydrogen scale (~4.5 eV); E_g was the band gap of the semiconductor, and the E_{VB}^{0} can be calculated by $E_{VB}^{0} = E_{CB}^{0} + E_g$.[18,24] The predicted band edge positions of Bi_2O_3 and $BaTiO_3$ by the above equation were shown in Table 1.

Figure 7 showed the CPDs of Bi_2O_3 and $BaTiO_3$ obtained by the Kelvin probe. The surface work functions of Bi_2O_3 and $BaTiO_3$ were 5.04 and 5.14 eV, respectively. On the basis of the

Table 1. Absolute Electronegativity, Estimated Band Gap, Energy Levels of Calculated Conduction Band Edge, and Valence Band at the Point of Zero Charge for Bi_2O_3 and $BaTiO_3$

semiconductor oxides	absolute electronegativity (X)	E_g (eV)[a]	conduction band edge (eV)	valence band edge (eV)
$BaTiO_3$	5.242	3.18	−0.84	2.34
Bi_2O_3	5.986	2.38	0.29	2.67

[a] $E_g = 1240/\lambda$, calculated using SPV data.

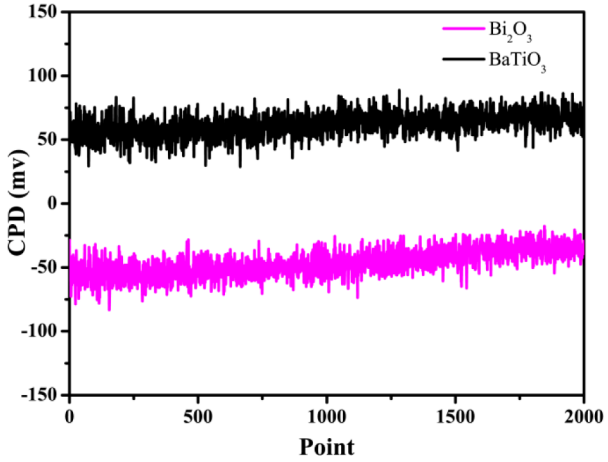

Figure 7. CPDs of pure Bi_2O_3 and $BaTiO_3$ related to the Au reference probe.

results, we could deduce that the Fermi level of Bi_2O_3 was 0.1 eV higher than that of $BaTiO_3$. It is well-known that two semiconductors with different work functions contact each other, charge would be transferred between them until have the same Fermi levels.[25] Thus, the electrons in Bi_2O_3 would transfer to the $BaTiO_3$ when they come to contact, the junction with SCR formed as shown in Figure 8b.

We speculated the photocatalytic mechanism of the composite as follow. Under the UV light irradiation (shown in Figure 8c), the photoinduced charge transfer process would occur between $BaTiO_3$ and Bi_2O_3 because of the interfacial electric field. With the aid of interfacial electric field, photoinduced electrons in conduction band of $BaTiO_3$ can

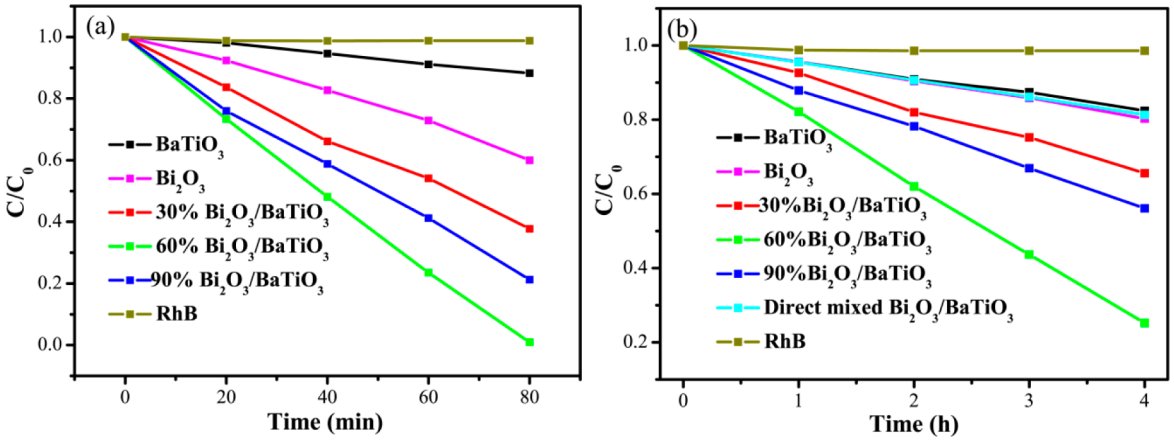

Figure 6. Kinetics of photodegradation of RhB by using $BaTiO_3$, Bi_2O_3 and Bi_2O_3/$BaTiO_3$ with different mass ratio under (a) UV light and (b) visible light (λ > 400 nm).

dx.doi.org/10.1021/am301199v | ACS Appl. Mater. Interfaces 2012, 4, 4853−4857

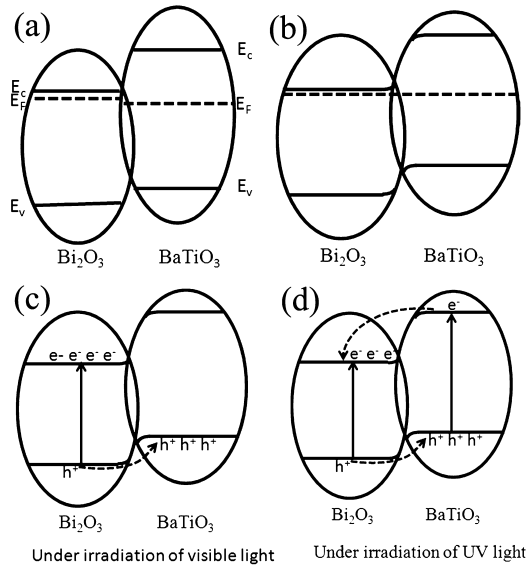

Figure 8. Schematic of (a) the conduction band and valence band potentials of Bi_2O_3 and $BaTiO_3$, (b) junction formation in a Bi_2O_3 /$BaTiO_3$ composite photocatalysts, and (c, d) the transfer direction of photoinduced charge under the irradiation of (c) visible and (d) UV light.

easily transfer to the conduction band of Bi_2O_3. At the same time, photoinduced holes in valence band of Bi_2O_3 transferred to $BaTiO_3$. This allowed Bi_2O_3 to scavenge electrons photoinduced in $BaTiO_3$ to stabilize the charge separation, and thus improved the photocatalytic activity of composite in degradation of RhB. Under the visible light irradiation, the composite with Bi_2O_3 as photosensitizer can absorb visible light. Under the effect of interfacial electric field, the photoinduced holes in the valence band of Bi_2O_3 moved to the valence band of $BaTiO_3$, and electrons stayed in Bi_2O_3, so the composite had the visible photocatalytic activity. However, when the mass ratio of Bi_2O_3 reached to 90 wt %, the photocatalytic activity of composite was weakened because the agglomeration of the Bi_2O_3 particles resulted in a reducing of photons reaching to the interface and an increasing of migration distance of photoinduced charges.

4. CONCLUSION

In summary, the as-prepared Bi_2O_3/$BaTiO_3$ composites show better photocatalytic activity than pure Bi_2O_3 or $BaTiO_3$ photocatalyst in degrading RhB. The notably high activity originates from the improvement of the separation efficiencyof photoinduced charge under the effect of interfacial electric field, which is established by the suitable relative band positions of these two semiconductors and obtaining their effective interfacial contact by impregnating-annealing method.

AUTHOR INFORMATION

Corresponding Author

*E-mail: xietf@jlu.edu.cn. Tel: +86 431 85168093.

Notes

The authors declare no competing financial interest.

ACKNOWLEDGMENTS

We are grateful to the National Natural Science Foundation of China (21173103, 51172090) and the Science and Technology Developing Funding of Jilin Province (201115012) for the financial support.

REFERENCES

(1) Subramanian, V.; Wolf, E. E.; Kamat, P. V. *J. Am. Chem. Soc.* **2004**, *126*, 4943.
(2) Lei, Z.; You, W.; Liu, M.; Zhou, G.; Takata, T.; Hara, M.; Domen, K.; Li, C. *Chem. Commun.* **2003**, *11*, 2142.
(3) Liu, G.; Zhao, Y.; Sun, C.; Li, F.; Lu, G. Q.; Cheng, H.-M. *Angew. Chem., Int. Ed.* **2008**, *47*, 4516.
(4) Wang, P.; Huang, B.; Zhang, X.; Qin, X.; Dai, Y.; Jin, H.; Wei, J.; Whangbo, M.-H. *Chem.—Eur. J.* **2008**, *14*, 10543.
(5) Gao, X. F.; Sun, W. T.; Hu, Z. D.; Ai, G.; Zhang, Y. L.; Feng, S.; Li, F.; Peng, L. M. *J. Phys. Chem. C* **2009**, *113*, 20481.
(6) Gao, B.; Kim, Y. J.; Chakraborty, A. K.; Lee, W. I. *Appl. Catal. B: Environ.* **2008**, *83*, 202.
(7) Zhai, J. L.; Wang, L. L.; Wang, D. J.; Li, H. Y.; Zhang, Y.; He, D. Q.; Xie, T. F. *ACS Appl. Mater. Interfaces* **2011**, *3*, 2253.
(8) Arai, T.; Yanagida, M.; Konishi, Y.; Iwasaki, Y.; Sugihara, H.; Sayama, K. *J. Phys. Chem. C* **2007**, *111*, 7574.
(9) Long, M.; Cai, W. M.; Cai, J.; Zhou, B. X.; Chai, X. Y.; Wu, Y. H. *J. Phys. Chem. B* **2006**, *110*, 20211.
(10) Hameed, A.; Montini, T.; Gombac, V.; Fornasiero, P. *J. Am. Chem. Soc.* **2008**, *130*, 9658.
(11) Guan, M. L.; Ma, D. K.; Hu, S. W.; Chen, Y. J.; Huang, S. M. *Inorg. Chem.* **2011**, *50*, 800.
(12) Huang, H. J.; Li, D. Z.; Lin, Q.; Zhang, W. J.; Shao, Y.; Chen, Y. B.; Sun, M.; Fu, X. Z. *Environ. Sci. Technol.* **2009**, *43*, 4164.
(13) Lin, X. P.; Xing, J. C.; Wang, W. D.; Shan, Z. C.; Xu, F. F.; Huang, F. Q. *J. Phys. Chem. C* **2007**, *111*, 18288.
(14) Chen, H.-J.; Chen, Y.-W. *Ind. Eng. Chem. Res.* **2003**, *42*, 473.
(15) Kim, H. W.; Na, H. G.; Yang, J. C.; Kim, H. S.; Lee, J.-H.; Yoo, K.-H. *Electrochem. Solid-State Lett.* **2010**, *13*, K67.
(16) Zhu, X.; Zhang, Z.; Zhu, J.; Zhou, S.; Liu, Z. *J. Cryst. Growth* **2009**, *311*, 2437.
(17) Gobrecht, H.; Seeck, S.; Bergt, H. E.; Märtens, A.; Kossmann, K. *Phys. Status Solidi* **1969**, *33*, 599.
(18) Xu, Y.; Schoonen, M. A. A. *Am. Mineral.* **2000**, *85*, 543.
(19) Zhao, Q. D.; Xie, T. F.; Peng, L. L.; Lin, Y. H.; Wang, P.; Peng, L.; Wang, D. J. *J. Phys. Chem. C* **2007**, *111*, 17136.
(20) Wei, X.; Xie, T. F.; Peng, L. L.; Fu, W.; Chen, J. S.; Gao, Q.; Hong, G. Y.; Wang, D. J. *J. Phys. Chem. C* **2011**, *115*, 8637.
(21) Bessekhouad, Y.; Robert, D.; Weber, J. V. *Catal. Today* **2005**, *101*, 315.
(22) Xie, T. F.; Wang, D. J.; Chen, S. M.; Li, T. J. *Thin Solid Films* **1998**, *327–329*, 415.
(23) Liu, Z. Y.; Sun, D. D. L.; Guo, P.; Leckie, J. O. *Nano Lett.* **2007**, *7*, 1081.
(24) Butler, M. A.; Ginley, D. S. *J. Electrochem. Soc.* **1978**, *125*, 228.
(25) Kronik, L.; Shapira, Y. *Surf. Sci. Rep.* **1999**, *37*, 1.